Applications of ultraviolet photofunctionalized titanium to bone regenerative medicine

Manabu Ishijima

Nihon University Graduate School of Dentistry,

Major in Partial Denture Prosthodontics

(Directors: Prof. Tomohiko Ishigami and Assoc. Prof. Naoki Tsukimura)

Table of Contents

Page

The following two articles are part of this doctoral dissertation:
    Journal of Biomaterials Applications (in press)
    Biomedical Research (in press)

Abstract

Active research into bone regenerative medicine has recently aimed to overcome the defects caused by trauma, congenital defects, and tumor excision. However, many issues need to be addressed to obtain a satisfactory outcome. In particular, ultraviolet photofunctionalization of the surface of titanium is known to be an effective surface conditioning method for obtaining a higher affinity for osteoblasts. Photofunctionalization is defined as a surface treatment that uses ultraviolet light at a specific wavelength and strength. This technology is used in dental implants because of the induced affinity for osteoblasts and the achievement of stronger osseointegration. Titanium is also used in bone regenerative medicine, but photofunctionalization has not been applied in this field. In the present study, photofunctionalization was applied to bone regenerative medicine.

In the first chapter, the establishment of titanium-reinforced cell sheets which comprised cell sheets with a thin titanium mesh was described. These titanium-reinforced cell sheets were produced to overcome the disadvantages of cell sheets in terms of physical strength by adding a titanium framework. The technical requirements and appropriate conditions of the materials were assessed. Cell sheets of rat calvarial periosteum-derived cells were attached to a titanium plate and their structural stability and functional phenotype were assessed. To establish a structurally stable complex that comprised cell sheets and titanium framework, a method where a single cell sheet was attached to one side of the titanium plate and another method where cell sheets were attached to both sides of the titanium plate were compared. Stable complexes were established using a sandwich technique where cell sheets were attached to both sides of the titanium plates. In addition, photofunctionalization of the titanium plates was critical to obtain the required stability. Photofunctionalization significantly enhanced the attachment of cell sheets to the titanium plates. The titanium-reinforced cell sheets established using a combination of the sandwich technique and photofunctionalization allowed the development of the expected osteogenic phenotypes (alkaline phosphatase production and mineralization), as well as maintenance the structural integrity without functional degradation. The mechanism of enhanced cell sheet attachment to titanium plates may be explained by the amount of protein absorption that occurred prior to cell attachment and expression of the adhesion protein vinculin. The amount of absorbed protein and vinculin expression were increased by photofunctionalization.

In the second chapter, an examination of the effect of photofunctionalization on titanium scaffolds that comprised micro-thin titanium fibers was described. Titanium scaffolds with

and without photofunctionalization were seeded using rat bone marrow-derived osteoblasts, before examining the number of cells that attached to the scaffolds and the osteoblastic phenotype in cultures. Photofunctionalization improved the wettability of the scaffolds and significantly reduced the percentage of surface carbon. In addition to these physicochemical changes in the scaffolds, the extent of cell attachment were increased compared with that in the untreated control. Furthermore, the alkaline phosphatase activity and calcium deposition were significantly increased. Robust mineralized structures that comprised clear peaks of calcium and phosphorus were formed in the photofunctionalized scaffolds.

The present study examined the possibility of the application of ultraviolet photofunctionalization to bone regenerative medicine using two different methods. The establishment of titanium-reinforced cell sheets and photofunctionalized titanium scaffolds demonstrate the potential utility of photofunctionalization in bone regenerative medicine.

Chapter 1:

Osteogenic cell sheets reinforced with photofunctionalized micro-thin titanium

Manabu Ishijima, Makoto Hirota, Wonhee Park, Masaki J. Honda

Naoki Tsukimura, Keitaro Isokawa, Tomohiko Ishigami, Takahiro Ogawa

Introduction

Bone engineering, or bone regeneration therapy, is a promising alternative to conventional reconstructive surgery in the treatment of cancer, injury, and degenerative disease in bone and joints, which are increasing in incidence in our aging society[1-4]. However, bone engineering faces a number of unsolved challenges, including difficulties in regenerating large volumes of bone, ensuring mechanical tolerance, and shaping regenerating bone. These challenges mainly arise from an insufficient supply of osteogenic cells, the limited functional capacity of the cells, and a lack of structural and mechanical integrity between scaffolds and regenerated bone [5-13].

Cell sheet technology was developed to effectively and efficiently regenerate tissue using a seamless mixture of cells and extracellular matrix (ECM)[14-16]. Using a specialized culture dish, a cell-ECM complex can be harvested in sheet form [17-19]. Cell sheet technology is superior to conventional cell suspension techniques due to its technical feasibility (a large number of cells can be transplanted at a time), and, in general, a larger proportion of cells survive transplantation and maintain their functional phenotypes and structural integrity due to the preservation of cell-cell and cell-ECM contacts. Cell sheet harvesting is non-enzymatic, non-invasive, and relies on the hydrophobic to hydrophilic conversion of poly (N-isopropylacrylamide) (PIPAAm), a temperature-responsive polymer [15, 16]. When coated with PIPAAm, the culture dish is hydrophobic at 37ºC but changes to hydrophilic below 32ºC. Therefore, cells that have reached confluency on PIPAAm dishes at 37ºC start to dissociate from the dish surface as an intact layer when the temperature drops below 32ºC. The technology has been used in a variety of experimental and clinical applications in different organs and tissues such as the skin, heart, liver, cornea, ligaments, cartilage, and bone [15, 16, 20-26]. However, the application and efficacy of cell sheet technology are limited to the repair of superficial or small parts of organs, or to regeneration at the tissue, rather than organ, level. Application to bone tissue has been particularly challenging due to the need to regenerate massive amounts of mechanically stable tissue.

Photofunctionalization is an emerging technology in which titanium surfaces are activated by treatment with ultraviolet (UV) light immediately prior to use, and has been clinically

proven effective in dental implants [27-34]. Photofunctionalized titanium surfaces are hydrophilic, electropositive, and minimally contaminated with hydrocarbons, whereas as-received or untreated titanium surfaces are hydrophobic, electronegative, and significantly contaminated with hydrocarbons from the atmosphere [32, 35-38]. The photofunctionalized physicochemical changes result in a three-fold increase in bone-titanium integration strength compared to untreated control titanium, and bone-titanium implant contact is 98.2% for photofunctionalized implants compared to 53% for untreated implants [29, 32].

In this present study a potential use of cell sheets with photofunctionalized titanium in bone engineering was examined. It was hypothesized that titanium can be used as a framework to stabilize and accommodate the construction and safe delivery of shaped cell sheets. The objective of this study was to construct titanium-reinforced osteogenic cell sheets and examine their structural stability and functional phenotype for potential use in bone engineering and regeneration.

Materials and methods

Titanium framework and photofunctionalization

A micro-thin titanium plate with a mesh structure was used as a candidate framework to support cell sheets. The titanium plate was made of commercially pure titanium (ACE Surgical, Brockton, MA) and contained circular apertures (0.8 mm diameter) evenly and regularly distributed within the 50 μm thick plate. The calculated aperture ratio, relative to the surface area of titanium, was 40.0%. This titanium plate was cut into circular form (5 mm diameter) and acid-etched with 67% (w/w) sulfuric acid (H_2SO_4) at 120°C for 75 s prior to storage in the dark for four weeks to standardize the age of the titanium, since titanium age is known to affect its biological and osteoconductive capabilities [39, 40]. The surface morphology and chemistry were examined using scanning electron microscopy (SEM) (XL30, Philips, Eindhoven, Netherlands) and X-ray photoelectron spectroscopy (XPS) (ESCA3200, Shimadzu, Tokyo, Japan), respectively. The hydrophilic and hydrophobic properties of the titanium plates were evaluated by measuring the contact angle of 10 μl of ddH_2O. Photofunctionalization was performed by treating the micro-thin titanium plates with UV light for 12 min using a photo device (TheraBeam SuperOsseo, Ushio Inc, Tokyo, Japan) immediately prior to use in cell culture experiments.

Osteogenic cell culture

Periosteal cells were isolated from the calvarial periostea of eight-week-old male Sprague-Dawley rats as previously reported [33, 41]. After sacrificing the animals, the calvarial

bone was extracted aseptically. After washing with 1% phosphate buffered solution (PBS, MP Biomedicals, Solon, OH, USA), the periosteum was collected by scraping the bone surface using a scalpel. The tissue was then dissected into small pieces (<1 mm^2) and digested with 0.25% collagenase for 1 h. The liberated cells were collected and plated in a 100 mm tissue culture dishes with alpha-modified Eagle's medium supplemented with 15% fetal bovine serum, 50 µg/ml ascorbic acid, 10 mM Na-β-glycerophosphate, 10^{-8} dexamethasone, and antibiotic-antimycotic solution in a humidified atmosphere of 95% air and 5% CO_2 at 37°C. At 80% confluency, the cells were detached using 0.25% trypsin 1 mM EDTA-4Na and seeded onto temperature-responsive culture dishes (UpCell, CellSeed, Tokyo, Japan) at a concentration of 2×10^4 cells/cm^2. The culture medium was renewed every three days.

Construction of titanium-reinforced osteogenic cell sheets

The step-by-step protocol for construction of titanium-reinforced osteogenic cell sheets is shown in Figure 1. Periosteal cell sheets were prepared non-enzymatically as recommended by the manufacturer. Briefly, periosteal cells cultured in temperature-responsive dishes for seven days and at confirmed confluency were removed from the incubator and kept at room temperature. As the temperature dropped from 37°C to 25°C (after about 10-15 minutes), the cells started to dissociate from the dish as a sheet.

Titanium-reinforced osteogenic cell sheets were constructed using two different techniques: single-sided and double-sided (Figure 1). For single-sided cell sheets, a titanium plate was placed on a periosteal cell sheet about to detach from a temperature-responsive culture dish. The titanium plate was left for five min to allow the formation of a titanium-cell sheet complex. After complexation, the titanium-cell sheet complex was transferred to a regular culture-grade polystyrene dish for further experiments with the cell sheet facing up and the titanium plate facing down.

Double-sided cell sheets were prepared by extension of the single-sided technique (Figure 1). A periosteal cell sheet was prepared on a temperature-responsive culture dish and, when the cell sheet was about to detach at 25°C, a pre-constructed single-sided cell sheet was placed onto the new cell sheet with the exposed titanium facing it. After five min, the double-coated titanium-cell sheet complex was transferred to a regular polystyrene culture dish for further experiments. Both photofunctionalized and non-photofunctionalized (untreated) titanium plates were tested for titanium-cell sheet complexation using both single- and double-sided methods.

Titanium-cell sheet retention test

The coverage of cell sheets relative to the total area of the titanium plate was measured at the time of titanium-cell sheet complexation and 24 h later using image analysis software (ImageJ, NIH, Bethesda, ML). The titanium-cell sheet retention was calculated as [(cell sheet coverage after 24 h)/(cell sheet coverage at construction)]×100 (%). When part of the cell sheet detaches from the titanium plate or rolls up, the titanium-cell sheet retention will be less than 100%.

Adhesion behavior of cell sheets on micro-thin titanium

Confocal laser scanning microscopy was used to assess the adhesion behavior of cell sheets on titanium plates. Since titanium-cell sheet retention testing showed very poor retention of cell sheets using the single-sided technique, adhesion behavior was only examined for double-sided sheets. Twenty-four hours after construction of a double-sided titanium-cell sheet complex, cell sheets were fixed in 10% formalin and stained using rhodamine phalloidin fluorescent dye (actin filament, red color; Molecular Probes, OR). In addition, cell sheets were stained with mouse anti-vinculin monoclonal antibodies (Abcam, Cambridge, MA), followed by FITC-conjugated anti-mouse secondary antibodies (Abcam) to visualize the expression of vinculin, a focal adhesion protein. The intensity of actin and vinculin expression per unit area was quantified using image analysis software (ImageJ, NIH, Bethesda, ML). Cross-sectional images were also obtained to examine the localization of vinculin at the titanium-cell sheet interface.

Alkaline phosphatase (ALP) activity

Image- and colorimetry-based analyses were used to detect the ALP activity of titanium-reinforced cell sheets on days 0 and 7 of culture. Cell sheets were washed twice with Hanks' solution and incubated with 120 mM Tris buffer (pH 8.4) containing 0.9 mM naphthol AS-MX phosphate and 1.8 mM fast red TR for 30 min at 37°C. The areas of cell sheets within the apertures were examined under a microscope. As a colorimetry-based assay, cultures were rinsed with ddH$_2$O and 250μl p-nitrophenylphosphate was added (LabAssay ATP, Wako Pure Chemicals, Richmond, VA) before being incubated at 37°C for 15 min. The ALP activity was evaluated as the quantity of nitrophenol released via the enzymatic reaction and measured at a wavelength of 405 nm using a plate reader.

Mineralization assay

The mineralization capability of titanium-reinforced cell sheets was examined by visualizing mineralized nodule areas and measuring the amount of calcium deposition. Alizarin red staining was used to visualize nodule areas: on days zero and 14 of culture, the specimens were washed twice with 1X PBS at 37°C and stained for five min using 1%

Alizarin red (pH 6.3-6.4). The specimens were then rinsed twice with distilled water and air dried for microscopic examination. For colorimetric detection of calcium deposition, cultures were washed with PBS and incubated overnight in 1 ml of 0.5 M HCl solution with gentle shaking. The solution was mixed with o-cresolphthalein complexone in alkaline medium (Calcium Binding and Buffer Reagent, Sigma, St Louis, MO) to produce a red calcium-cresolphthalein complexone complex. Color intensity was measured using a plate reader (Synergy HT, BioTek Insturuments, Winooski, VT) at 575 nm.

Biological characterization of photofunctionalized titanium

Based on the successful construction of titanium-reinforced cell sheets on photofunctionalized titanium plates only, protein adsorption and the attachment, retention, and initial settling behavior of periosteal cells were assayed to compare the bioactivity of untreated and photofunctionalized titanium plates.

Protein adsorption

Bovine serum albumin (BSA; Pierce Biotechnology, Inc., Rockford, IL) was used as a model protein. Three hundred μl of protein solution (1 mg/ml protein/saline) was pipetted over a titanium plate. After six and 24 hours of incubation in sterile humidified conditions at 37°C, the solution containing non-adherent proteins was removed and mixed with micro bicinchoninic acid (BCA; Pierce Biotechnology) at 37°C for 60 min. The quantity of removed and total protein was measured using a microplate reader (Synergy HT, BioTek Instruments, Winooski, VT) at 562 nm. Protein adsorption was calculated as the percentage of protein adsorbed to the titanium plate relative to the total amount.

Cell attachment assay

The capability of untreated and photofunctionalized titanium plates to attract cells was evaluated by measuring the number of cells attached to a titanium plate after 24 h of incubation with periosteal cells using WST-1-based colorimetry (WST-1, Roche Applied Science, Mannheim, Germany). The culture was incubated with 100 μl tetrazolium salt (WST-1) reagent at 37°C for four h. The amount of formazan produced was measured using an ELISA reader at 420 nm.

Cell retention assay

The retention of cells attached to the titanium plate was evaluated by calculating the percentage of remaining cells after enzymatic and mechanical detachment as previously described [42]. Periosteal cells incubated on titanium plates for 24 h were rinsed once with PBS to remove non-adherent cells, and then detached from the titanium plate by treating with

0.05% v/v trypsin-EDTA at 37°C for one min while vibrating a culture dish (amplitude 10 μm, frequency 30 Hz). The number of detached and remaining cells was quantified using the WST-1 assay as described above.

Cellular morphology and vinculin expression

Confocal laser scanning microscopy was used to assess the spreading and adhering behaviors of periosteal cells seeded on titanium plates. Cells were stained to detect actin and vinculin 24 h after seeding as described earlier. The area, perimeter, Feret's diameter, and intensity of vinculin expression per cell were quantified using image analysis software (ImageJ, NIH, Bethesda, ML).

Statistical analysis

All culture studies were performed in triplicate, except for cell morphometry and densitometry (n = 6). One-way ANOVA was used to examine differences between untreated (non-photofunctionalized) and photofunctionalized titanium groups, or between the different days of culture; $p < 0.05$ was considered statistically significant.

Results

Surface properties of micro-thin titanium plates with or without photofunctionalization

Low-magnification SEM showed that the titanium plate had uniform roughness as typically seen on acid-etched titanium (Figure 2A, left image). High-magnification images revealed a microscale compartmental morphology consisting of sharp peaks and valleys (Figure 2A, right image). Wettability testing revealed a drastic change after photofunctionalization (Figure 2B). Untreated titanium plates were hydrophobic with a ddH_2O contact angle greater than 90 degrees, whereas photofunctionalized titanium plates were hydrophilic with a ddH_2O contact angle of 0 degrees. XPS chemical analysis showed a significant reduction in the atomic percentage of carbon on photofunctionalized titanium plates (13.7%) compared to untreated plates (57.0%). A significant reduction in the elemental peak of carbon was also observed on photofunctionalized titanium plates (Figure 2C).

Cell sheet retention on micro-thin titanium

Immediately after construction of single-sided titanium-cell sheet complexes, a cell sheet layer was successfully retained on the titanium plate with or without photofunctionalization (Figure 3A, top images). However, the single-sided cell sheet deformed and detached from the titanium plate over the next 24 h of incubation regardless of photofunctionalization, exposing

the majority of the titanium plate (Figure 3A, bottom images). Cell sheet retention was less than 25% for both untreated and photofunctionalized titanium plates (Figure 3B).

Then, whether the double-sided cell sheet technique improved cell sheet retention was examined. Double-sided placement of cell sheets was technically feasible using the protocol described in Figure 1. Immediately after construction, the entire surface of both untreated and photofunctionalized titanium plates were covered by sandwiching cell sheets (Figure 4A, top images). After 24 h of incubation, most of the double-sided cell sheets remained intact and attached to photofunctionalized titanium plates, whereas approximately half the cell sheet area rolled up by contraction, deformation, or detachment on untreated titanium plates (Figure 4A, bottom images). Cell sheet retention at 24 h was 83% for photofunctionalized titanium plates and 60% for untreated titanium plates (p < 0.05).

Cell sheet integrity on titanium

Cell sheet-titanium plate integrity was evaluated. Since single-sided cell sheets were ineffective at 24 h, cell sheet integrity analysis was only conducted for double-sided cell sheets. Confocal microscopic images showed that the expression of vinculin, an adhesion protein, was generally upregulated in the cell sheets on photofunctionalized titanium plates compared to untreated titanium plates, whereas the expression of actin was similar between the two titanium plates (Figure 5A). Densitometric analysis of the confocal microscopic images confirmed greater expression of vinculin per unit area of cell sheet on photofunctionalized titanium plates (Figure 5B). There was no difference in vinculin or actin expression in the cell sheet within apertures (Figure 5C), confirming that the photofunctionalization effect is only apparent on the titanium surface. Lastly, merged cross-sectional images of actin and vinculin expression across the titanium plate showed more intense expression of vinculin at the photofunctionalized titanium-cell sheet interface, confirming the upregulated expression of vinculin in three dimensions (Figure 5D).

Functional phenotype of titanium-reinforced osteogenic cell sheets

To examine the maintenance of cell sheet-titanium integrity over longer periods of time and the phenotype of periosteal cells, double-sided titanium-cell sheet complexes were cultured for up to fourteen days. By day four, all double-sided cell sheets placed on untreated titanium plates shrank or rolled up (Figure 6A). In contrast, double-sided cell sheets on photofunctionalized titanium plates maintained their flat, spread, and intact morphology (Figure 6A). Therefore, functional assays were only performed on the double-sided cell sheets on photofunctionalized titanium. ALP activity was significantly greater at day 7 than on day 0 (Figure 6B and C). Alizarin red staining performed on day 14 showed that the cell sheets were

9

undamaged, with no tissue voids or defects observed on photofunctionalized titanium (Figure 7A). The cell sheets were stained positively for mineralized nodules on day 14 (Figure 7B) and was much greater than on day 0 (Figure 7B and C). These results confirmed that the cells developed their expected osteogenic functional phenotype.

Biological capability of photofunctionalized titanium plates

Protein and cellular assays were next conducted to explore the biological properties of photofunctionalized titanium plates contributing to the successful construction of titanium-reinforced osteogenic cell sheets. The amount of albumin adsorption after 6 and 24 h was significantly greater on photofunctionalized titanium plates than on untreated plates (Figure 8A). The number of attached cells after 24 h of incubation was also significantly greater on photofunctionalized titanium plates (Figure 8B). Over three-times more cells remained attached to photofunctionalized titanium plates after chemical and mechanical detachment than to untreated plates (Figure 8C). Cell spread was wider with greater expression of vinculin on photofunctionalized titanium plates than untreated titanium plates after 24 h (Figure 8D).

Discussion

In this present study, the feasibility of constructing titanium-reinforced osteogenic cell sheets were demonstrated. Cell sheets maintained their original form and surface area on flat, micro-thin titanium plates for at least 14 days and could safely be transferred from dish to dish. Cell sheets usually need to be detached from temperature-responsive dishes as soon as the cells reach confluence, otherwise they may dissociate voluntarily, and harvested cell sheets cannot be kept unused in their sheet form since they immediately roll up or shrink to form pellets. In addition to the successful construction of mechanically-reinforced cell sheets, this study demonstrates a possible method for storing cell sheets on titanium plates, which are easy to handle and may be transferred with controlled form and size. Although cells adhere to soft tissue organs when in sheet form, they are more resistant to settling on bone. The proposed titanium frame may be useful to engage surrounding bone to fix the cell sheet and for providing space-making and form-shaping functions. In addition, micro-thin titanium plates can be cut and adjusted to any form or size. The cell sheets manifested the expected osteogenic functional phenotype (ALP expression and mineralization), demonstrating that they were not significantly damaged or dedifferentiated during preparation.

The construction of titanium-reinforced osteogenic cell sheets was conditional, and a number of requirements must be met to achieve sustainable structural and functional integrity.

First, the cell sheet coverage needed to be double-sided. The structural integrity of single cell sheets on titanium was limited and failed to maintain cell sheet spread, indicating that titanium-cell sheet adhesion alone was insufficient for cell sheet retention, and cell sheet-cell sheet contact was necessary.　This problem was overcome by sandwiching a titanium plate between two cell sheets and allowing them to adhere via the apertures to create the titanium-cell sheet complex. Since the presence of apertures was a requirement for successful complexation, the size and density of apertures may also be important criteria for sufficiently retaining the cell sheets. Here, the aperture ratio of 40% was effective, but further optimization may be needed depending upon the cell type and application. Second, although comparative data are not available, the use of micro-thin titanium plates (rather than thick titanium plates) may have contributed to successful cell sheet retention by enabling close apposition of the two cell sheets. Third, the surface topography of the titanium may have played a role in complex integrity. Micro-scale roughness created by sandblasting, acid-etching, oxidation, titanium plasma-spray, or other methods has been used to create endosseous implant surfaces in dental and orthopedic surgery [43-48]. Compared to smoother, machined surface or polished titanium surfaces, the adhesion and retention of osteoblastic cells on rough surfaces are enhanced due to the increased surface area and cell-titanium interlocking [49, 50]. Since such surface roughening is easily achieved, it is recommended for secure construction. Finally, photofunctionalization was a critical factor; without photofunctionalization, double-sided cell sheet complexes only had a lifespan of less than four days, which was too short establish a useful functional phenotype. Photofunctionalized titanium, the advantage of which was shown in a series of protein and cellular experiments [51, 52], enabled the production of stable and durable titanium-reinforced cell sheets. Confocal microscopy showed that the expression of the vinculin adhesion protein was upregulated on photofunctionalized titanium surfaces at both the cell and cell sheet level, which may have contributed to cell sheet retention. It was confirmed that the vinculin was intensely and intimately localized at the titanium-cell sheet interface, as shown by cross-sectional confocal microscopic analysis. Probably as a result of this, cell retention on photofunctionalized titanium plates was three times greater than untreated titanium plates under harsh chemical and mechanical detachment conditions. Photofunctionalization appeared to increase the structural and mechanical integrity of cell sheet-titanium complexes.

The mechanisms underpinning the enhanced biological capability of photofunctionalized titanium are assumed to be due to the alteration in physicochemical properties, namely restored superhydrophilicity, decontamination of accumulated hydrocarbon, and positively converted electrostatic charge [29, 32, 37]. The increased hydrophilicity may prevent the formation of air bubbles at the titanium-cell sheet interface and allow complete contact. The exposure of

pure, hydrocarbon-free titanium may improve cellular behavior and response by improving cell and tissue adhesion at the titanium surface. Since the cell membrane is negatively charged, positively-charged titanium surfaces recruit more cells [29, 33, 36, 39, 52].

The construction of a novel osteogenic device has been made possible using photofunctionalization. Aperture-containing titanium plates, as used in this study, are commercially available and easily shaped, and the size and thickness can be controlled. In vivo studies are warranted from the perspective of developing novel osteogenic devices for various applications in the bone regeneration field. Furthermore, the application of titanium-reinforced cell sheets is not limited to bone tissue; the step-by-step protocol provided in this study could be applied to other cell and tissue types. For instance, considerable efforts have been made to fabricate multi-layered cell sheet complexes for soft tissue regeneration to provide sufficient thickness of the sheet to meet the geometric requirements of the repairing sites. However, stacking sheets makes it more difficult to maintain structural and functional integrity. The results suggest that a multi-layered cell sheet could be constructed with an aid of a photofunctionalized titanium framework, with the titanium frame itself possibly providing much-needed thickness.

Chapter 2:

Enhancing osteoblast-affinity of titanium scaffolds for bone engineering by use of ultraviolet light treatment

Manabu Ishijima, Pooya Soltanzadeh, Makoto Hirota

Naoki Tsukimura, Tomohiko Ishigami, Takahiro Ogawa

Introduction

Surface conditioning of photofunctionalization immediately prior to use effectively and efficiently establishes an osteoblast-affinity surface [32, 37, 53]. Since the development of this technique, the technology has been applied to dental implants to facilitate satisfactory bone formation around the implants [27, 28, 30]. Using this technology, the bone implant contact (BIC) index (an index to evaluate bone formation around the implants) of photofunctionalized implants was 98.2% compared to 51.7% in that of the untreated control after a four-week healing period in a rat study [29]. The photofunctionalization induces various physicochemical changes to the surface of titanium as follows: 1) removing accumulating carbon, 2) converting the hydrophilicity from hydrophobic to hydrophilic, and 3) converting the electrical charge from electro-negative to electro-positive [32, 37, 39, 53]. These surface properties of photofunctionalized titanium are considered advantageous for osteoblast affinity [36, 54, 55]. Furthermore, photofunctionalization can be applied to all titanium devices of any design surface topography. Therefore, this effective and versatile technology potentially has wide applications to every titanium device that requires osteoblast affinity.

Titanium scaffolds are considered suitable biomaterials for bone engineering due to their high porosity, physical strength, biocompatibility, and osteoconductive properties [56-58]. Different manufacturing methods and modifications of the titanium scaffolds have been studied to improve their capacity for bone engineering [56, 57]; for example, coating of the surface with bioactive substrates is a common strategy used to enhance bone formation. Studies have shown that coating of the titanium surface with binding proteins, including phosphoproteins and with thin hydroxylapatite, achieved enhancement of bone formation and osteoblast activity, respectively [55, 59-61]. The modification of titanium surface topography is also a possible option, because surface topography promotes the proliferation and differentiation of osteoblasts [62, 63]. For instance, a micro-roughened titanium surface has an advantage over machined smooth surfaces, and results in enhanced osteoblastic differentiation and faster bone formation [62, 63]. An advanced, innovative in vitro bone engineering technique uses a combination of titanium scaffolds along with a bone-like extracellular matrix and the

flow perfusion culture system [64]. However, these techniques sometimes require complicated processes and may still be incapable of ensuring predictable results and guaranteed success.

Photofunctionalization-induced osteoblast-affinity of titanium in two-dimensional plate cultures is well studied, but the utility of the technique in three-dimensional cultures remains unclear. The effect of photofunctionalization on three-dimensional cultures using titanium scaffolds was examined to assess the possible use of surface conditioning for bone engineering. It was hypothesized that the photofunctionalized titanium scaffold can efficiently attract osteoblasts and create bone effectively in vitro. In the present study, titanium scaffolds with and without photofunctionalization were seeded with rat bone marrow-derived osteoblasts, following which the number of cells attached to the scaffolds and osteoblastic phenotype of the cultures were assessed. In addition, the morphology and chemistry of the biological structures formed on the scaffolds were evaluated.

Materials and methods

Preparation of titanium scaffolds and their characterization

Rectangular titanium scaffolds (5 mm × 5 mm and 3 mm thick) comprising thin fibers of 20 μm diameter with 87% porosity (Hi-Lex, Kobe, Japan) were prepared for this experiment (Figure 9A). All scaffolds were etched with 67% H_2SO_4 (Sigma-Aldrich, Missouri, USA) at 120°C for 10 sec to establish a micro-roughed surface. The pore structure and surface topography were examined using a scanning electron microscope (SEM; Nova 230 NanoSEM, FEI, Hillsboro, Oregon). The elemental composition on titanium surfaces was evaluated by electron spectroscopy for chemical analysis (ESCA). ESCA was performed using an X-ray photoelectron spectroscopy (XPS) (ESCA3200; Shimadzu, Tokyo, Japan) under high vacuum conditions (6×10^{-7} Pa). The wettability of the titanium scaffolds was evaluated by measuring the contact angle of 10 μL of double distilled water (ddH_2O) droplets. Photofunctionalization was performed by treating the titanium scaffolds with UV light for 12 min using a photo device (TheraBeam SuperOsseo; Ushio Inc., Tokyo, Japan) immediately prior to use in cell culture experiments.

Osteoblast culture and seeding

The bone marrow-derived mesenchymal stromal cells of 8-week-old male Sprague-Dawley rats (Charles River Laboratories, California, USA) were cultured in an osteogenic induction medium containing alpha-modified Eagle's medium (Invitrogen, California, USA) supplemented with 15% fetal bovine serum (Invitrogen), 50 mg/mL ascorbic acid (Sigma-Aldrich), 10 mM Na-β-glycerophosphate (Sigma-Aldrich), 10^{-8} M

dexamethasone (Sigma-Aldrich), and antibiotic–antimycotic solution (Invitrogen). Cells were incubated in a humidified atmosphere of 95% air and 5% CO_2 at 37°C. Titanium scaffolds with and without photofunctionalization were placed in 24 well plates, following which scaffolds in the cells of passage 2 were seeded with a 1 mL cell suspension including 5×10^4 cells/ml. The culture medium was renewed every 3 days.

Cell attachment assay

The ability of titanium scaffolds to attract cells was evaluated by measuring the number of cells attached to the scaffolds after 24 h of incubation. The numbers of cells were quantified using WST-1 based colorimetry. In brief, the culture was incubated at 37°C for 1 h with 100 μl WST-1 reagent (Roche Applied Science, Mannheim, Germany). After incubation, the wave length of 450 nm was measured by a plate reader (Synergy HT; BioTek Instruments, Winooski, VT). In addition, cells were labeled with rhodamine phalloidin (Life technologies, New York, USA) and observed using a laser microscope (SP-5; Leica, Wetzlar, Germany).

Alkaline phosphatase (ALP) activity

ALP activity was evaluated on day 4 by colorimetry-based assays. The culture was rinsed with ddH_2O and 250 μL p-nitrophenylphosphate (Lab Assay ATP; Wako Pure Chemicals, Richmond, VA) was added, following which incubation at 37°C for 15 min occurred. The ALP activity was evaluated as the amount of nitrophenol released through the enzymatic reaction and measured at the wave length of 405 nm using a plate reader (Synergy HT; BioTek Instruments, Vermont, USA).

Mineralization assay

The mineralization capabilities of cultures were evaluated on day 10 by colorimetry-based assays. The cultures were washed with ddH_2O and incubated overnight in 1 ml of 0.5 M HCl solution (Sigma-Aldrich) with gentle shaking. The solution was mixed with o-cresolphthalein complexone in an alkaline medium (LiquiColor; Srtanbio, Texias, USA) to produce a purple calcium–cresolphthalein complexone complex. Color intensity was measured by a plate reader at the wave length of 550 nm.

Biological structure formed on the scaffold

The morphologies and elemental composition of the biological structure formed on the scaffold on day 10 were evaluated by SEM and energy dispersive x-ray spectroscopy (EDS) (UltraDry EDS Detector and NORAN™ System 6; Thermo Fisher Scientific, Inc., Massachusetts, USA). The cultures were fixed and dried following a previously described method (29). In brief, the specimens were fixed with 2.5% glutaraldehyde solution

(Sigma-Aldrich) and 1% osmium tetroxide (Sigma-Aldrich), and subsequently dehydrated by sequential immersion in 30%, 50%, 75%, 90%, 95%, and 99% ethanol (Sigma-Aldrich). The immersion in 99% ethanol was repeated thrice. Samples dehydrated with ethanol were thoroughly substituted with *t*-butanol (Sigma-Aldrich) and subjected to drying under vacuumed conditions at 4°C. After drying, the samples were observed by SEM using the low vacuum mode. The elemental composition was analyzed by EDS. The EDS spectrums were randomly measured and average Ca/P ratio and Ca/titanium ratio were calculated (n = 6).

Statistical analyses

All culture studies were performed in triplicates (n = 6). One-way analysis of variance (ANOVA) was used to examine differences between the un-treated control and the photofunctionalized scaffolds. $p < 0.05$ was considered statistically significant.

Results

Characterization of Photofunctionalized titanium scaffolds

1) Surface topography, 2) elemental composition of the surface, and 3) wettability were assessed to confirm the photofunctionalization-induced physicochemical changes on titanium scaffolds. Low magnification SEM imagery of the titanium scaffolds showed randomly arranged titanium fibers distributed evenly. The distance between each titanium fiber was between 150 μm and 200 μm and the pore sizes were approximately uniform (Figure 9B). High magnification SEM imagery of the titanium scaffolds represented a uniform roughness feature comprising sharp ridges and pits at a micron-scale (Figure 9C). No topographical change occurred because of photofunctionalization (Data not shown here). Photofunctionalization significantly decreased the percentage of surface carbon on titanium scaffolds. The percentage of occupancy of carbon on titanium scaffolds was 31.8 ± 3.9% before photofunctionalization and 10.5 ± 1.6% after photofunctionalization (Figure 10A). Photofunctionalized scaffolds showed good wettability. The droplets of 10 μl of ddH$_2$O placed on an untreated scaffold were reflected and took a spherical shape. In contrast, the water drops were immediately absorbed into Photofunctionalized scaffolds (Figure 10B). The contact angle of water drops were 123.5° ± 2.5° in the untreated control and 0° in the Photofunctionalized scaffolds (Figure 10C).

Photofunctionalization-enhanced cell attraction and osteoblastic phenotype

The number of cells attached onto the scaffold in the culture after 24 h was observed by a laser microscope and quantified using a WST-1 colorimetric assay to evaluate the ability of titanium scaffolds to attract cells. The micrograph stained for actin showed the existence of

cells on the scaffold with the photofunctionalized scaffolds attracting more cells on their surfaces compared to that of the control (Figure 11A). The cells on the photofunctionalized scaffolds extended cell projections to a wider extent and displayed cell spreading along titanium fibers (Figure 11A). The WST-1 result supported the finding of the microscopic observation. Colorimetrically measured cell numbers in the photofunctionalized scaffolds were 30% higher than that of the untreated control (Figure 11B). In addition, ALP activity and the amount of calcium deposition were assessed as osteoblastic phenotypes. Photofunctionalized titanium scaffolds demonstrated a significant enhancement in the osteogenic phenotypes to a factor of 2.3 times in the ALP activity and 2.0 times in the calcium deposition as compared to those in the untreated control (Figure 11C, D).

Enhanced in vitro bone formation on the Photofunctionalized scaffolds

The in vitro biological structures formed on the titanium scaffolds were assessed to evaluate the ability of titanium scaffolds to facilitate substantial bone formation. The amount and quality of the biological structures formed on the scaffolds in the culture were assessed using SEM and EDS after 10 days. The mapping image of untreated and photofunctionalized scaffolds showed distinct elemental localization and element composition. The mapping image of the untreated control scaffold represented the elements of titanium as fibrous shapes and overlapping localization of calcium and phosphorus (Figure 12A). In contrast, almost all titanium fibers within the photofunctionalized scaffolds were covered by calcium and phosphorus (Figure 12A). The calcium/phosphorus ratio was calculated to evaluate the maturation of mineralized structures, and no significant difference was observed between the untreated control and the photofunctionalized scaffolds (Figure 12B). Photofunctionalized titanium scaffolds showed substantially higher values of the calcium/titanium ratio, representing the occupancy of calcium as compared to that of titanium on the surface of the specimens (Figure 12C).

In addition, the biological structures formed on the scaffolds represented clear morphological differences between untreated control and photofunctionalized scaffolds. Within the spaces between titanium fibers on the untreated control scaffolds, small amounts of biological structures were formed (Figure 13A). These structures were not enough to occupy spaces between fibers in untreated titanium scaffolds (Figure 13A). High magnification image showed matrix vesicles that were secreted by osteoblasts, and intact bare titanium surface was observed on untreated control titanium fibers (Figure 13B). In contrast, substantial biological structures filling the spaces between titanium fibers were formed on photofunctionalized scaffolds after the same period (Figure 13C, D). Photofunctionalized titanium fibers were fully covered by bone without a bare titanium surface (Figure 13E).

Discussion

The osteoblast affinity of photofunctionalized titanium surfaces is well studied in two-dimensional plate culture and has an impact in the research field of titanium implants, particularly in regards to the two-dimensional interface of biomaterials. For instance, the established BIC (Bone-Implant Contact) in photofunctionalized implants is approximately 100%, which is a result that has not been achieved by any other surface treatment method. The benefits of UV light treatment on titanium disks so as to achieve excellent bone formation with activated behavior of osteoblasts are as follows: 1) increased osteoblast migration; 2) increased attachment of osteoblasts; 3) facilitated osteoblast spread; 4) increased proliferation of osteoblasts; and 5) promoted osteoblastic differentiation [29]. In the present study, photofunctionalization in addition significantly enhanced cell attachment and osteoblastic phenotype on the three-dimensional culture with titanium scaffolds (Figure 11A–D). This study revealed for the first time the biological effect of photofunctionalization on the activation of osteoblast behavior in the three-dimensional culture. The substantial in vitro bone formation strongly suggested potential use of this photofunctionalization for the titanium scaffold based bone formation.

UV light treatment effectively removed carbon from the surface of the titanium scaffold used in this study (Figure 10A). Photofunctionalization significantly decreased the percentage of surface carbon to one third compared with that of untreated control. Previous study reported the influence of carbon accumulation to titanium surface on the osteoblast affinity [55]. In that study, behavior of osteoblasts cultured on titanium with different degrees of hydrocarbon contamination was observed. The suppression of initial cellular activities, such as cell attachment and cell spreading, was revealed in a concentration-dependent manner by the amount of carbon on the titanium surface. The present study also suggested the significant influence of carbon accumulation to the titanium scaffold on the osteoblast affinity. Removing the invisible carbon from the titanium device may be a key for successful titanium scaffold-based bone engineering.

Hydrophilicity is an important property for the scaffold, because it related with the efficiency with which liquid can move to the inside of scaffolds. In contrast, scaffolds with hydrophobic properties inhibit the movement of liquid into the scaffold. Penetration of cell suspension to the inside of the scaffolds is important in in vitro and penetration of blood and bone marrow to the inside of the scaffolds is important in in vivo. The photofunctionalized titanium scaffolds showed hydrophilic properties that were suitable for bone engineering

18

(Figure 10B, C). In addition, photofunctionalization is strongly recommended for application to a rough surface. While a rough surface has an advantage of promoting differentiation of osteoblasts [62, 63], this surface topography emphasizes the hydrophobic status of untreated titanium. As the Wenzel Equation indicates, hydrophilic surfaces become more hydrophilic, whereas hydrophobic surfaces become more hydrophobic with an increase in roughness [65]. The combined use of a rough surface and photofunctionalization might be the reasonable solution to achieve both promoted differentiation of osteoblasts and a hydrophilic property.

Scaffold materials suitable for bone engineering are required to possess the ability to attract cells to their surface because osteoblasts are anchorage-dependent cells that need an appropriate adhesion signaling to proliferate [54, 66, 67]. Photofunctionalization promotes cell attraction and adhesion through electrostatic mechanisms [36]. The mechanisms convert the electrical charge of titanium from electro-negative to electro-positive. An established electro-positive titanium surface is able to attract more cells because most cells are negatively charged [29, 32, 37, 53]. In the present study, photofunctionalized scaffolds attracted 30 % more cells to their surface as compared to the untreated control (Figure 11B). It is probable that the electrostatic mechanism might affect the cell attraction within this three-dimensional scaffold.

Robust formations of mineralized structures were observed in photofunctionalized scaffolds. EDS spectrum of this structure on photofunctionalized scaffolds showed a clear peak of calcium and phosphorus, and the average Ca/P ratio was 1.3:1 (Figure 12C). This Ca/P ratio is close to 1.66:1 of mature bone [68, 69]. The structures were almost filling the space between titanium fibers of the scaffold. Previous studies using similar titanium scaffolds reported calcified structures with large and small globular accretions and collagen bundles covered the fibers [70, 71], but the substantial mineralized structure filling the spaces between each fiber were not established. The substantial formation of mineralized structures in photofunctionalized scaffolds indicates the potential use of photofunctionalized titanium scaffolds for bone engineering.

Conclusion

The application possibility of photofunctionalization to bone regenerative medicine was assessed in this present study. Two different applications were tested and the following conclusions were obtained.

1. Titanium-reinforced osteogenic cell sheets were successfully constructed using photofunctionalization via photofunctionalization-induced enhanced cell attachment, retention, and expression of adhesion proteins.

2. Photofunctionalization enhanced formation of mineralized structures in the titanium scaffolds which used in bone engineering.

These results of in vitro experiments indicated the potential application of photofunctionalization for bone regenerative medicine. Future discussion and extra in vivo studies are required for further development of the study of photofunctionalization.

References

1.   Amini AR, Laurencin CT, Nukavarapu SP. Bone tissue engineering: recent advances and challenges. Crit Rev Biomed Eng 2012;40(5):363-408.

2.   Frost SA, Nguyen ND, Black DA, et al. Risk factors for in-hospital post-hip fracture mortality. Bone 2011;49(3):553-8.

3.   Takaoka S, Yamaguchi T, Tanaka K, et al. Fracture risk is increased by the complication of hypertension and treatment with calcium channel blockers in postmenopausal women with type 2 diabetes. J Bone Miner Metab 2013;31(1):102-7.

4.   Van den Bergh JP, van Geel TA, Geusens PP. Osteoporosis, frailty and fracture: implications for case finding and therapy. Nat Rev Rheumatol 2012;8(3):163-72.

5.   Bose S, Roy M, Bandyopadhyay A. Recent advances in bone tissue engineering scaffolds. Trends Biotechnol 2012;30(10):546-54.

6.   Lewandowska-Szumiel M, Wojtowicz J. Bone tissue engineering - a field for new medicinal products? Curr Pharm Biotechnol 2011;12(11):1850-9.

7.   O'Keefe RJ, Mao J. Bone tissue engineering and regeneration: from discovery to the clinic-an overview. Tissue Eng Part B Rev 2011;17(6):389-92.

8.   Schroeder JE, Mosheiff R. Tissue engineering approaches for bone repair: concepts and evidence. Injury 2011;42(6):609-13.

9.   Lu HH, Spalazzi JP. Biomimetic stratified scaffold design for ligament-to-bone interface tissue engineering. Comb Chem High Throughput Screen 2009;12(6):589-97.

10.   Hutmacher DW, Garcia AJ. Scaffold-based bone engineering by using genetically modified cells. Gene 2005;347(1):1-10.

11.   Razzouk S, Schoor R. Mesenchymal stem cells and their challenges for bone regeneration and osseointegration. J Periodontol 2012;83(5):547-50.

12.   Haidar ZS, Hamdy RC, Tabrizian M. Delivery of recombinant bone morphogenetic proteins for bone regeneration and repair. Part A: Current challenges in BMP delivery. Biotechnol Lett 2009;31(12):1817-24.

13.   Sreejit P, Verma RS. Natural ECM as biomaterial for scaffold based cardiac regeneration using adult bone marrow derived stem cells. Stem Cell Rev 2013;9(2):158-71.

14.   Matsuura K, Utoh R, Nagase K, et al. Cell sheet approach for tissue engineering and regenerative medicine. J Control Release 2014;190:228-39.

15.   Yang J, Yamato M, Shimizu T, et al. Reconstruction of functional tissues with cell sheet engineering. Biomaterials 2007;28(34):5033-43.

16.   Owaki T, Shimizu T, Yamato M, et al. Cell sheet engineering for regenerative medicine: current challenges and strategies. Biotechnol J 2014;9(7):904-14.

17.   Kumashiro Y, Matsunaga T, Muraoka M, et al. Rate control of cell sheet recovery by

incorporating hydrophilic pattern in thermoresponsive cell culture dish. J Biomed Mater Res A 2014;102(8):2849-56.

18. Patel NG, Zhang G. Responsive systems for cell sheet detachment. Organogenesis 2013;9(2):93-100.

19. Nagase K, Kobayashi J, Okano T. Temperature-responsive intelligent interfaces for biomolecular separation and cell sheet engineering. J R Soc Interface 2009;6 Suppl 3:S293-309.

20. Cerqueira MT, Pirraco RP, Martins AR, et al. Cell sheet technology-driven re-epithelialization and neovascularization of skin wounds. Acta Biomater 2014;10(7):3145-55.

21. Wu KH, Mo XM, Liu YL. Cell sheet engineering for the injured heart. Med Hypotheses 2008;71(5):700-2.

22. Hitani K, Yokoo S, Honda N, et al. Transplantation of a sheet of human corneal endothelial cell in a rabbit model. Mol Vis 2008;14:1-9.

23. Tani G, Usui N, Kamiyama M, et al. In vitro construction of scaffold-free cylindrical cartilage using cell sheet-based tissue engineering. Pediatr Surg Int 2010;26(2):179-85.

24. Nakamura A, Akahane M, Shigematsu H, et al. Cell sheet transplantation of cultured mesenchymal stem cells enhances bone formation in a rat nonunion model. Bone 2010;46(2):418-24.

25. Matsuura K, Masuda S, Shimizu T. Cell sheet-based cardiac tissue engineering. Anat Rec (Hoboken) 2014;297(1):65-72.

26. Elloumi-Hannachi I, Yamato M, Okano T. Cell sheet engineering: a unique nanotechnology for scaffold-free tissue reconstruction with clinical applications in regenerative medicine. J Intern Med 2010;267(1):54-70.

27. Funato A, Ogawa T. Photofunctionalized dental implants: a case series in compromised bone. Int J Oral Maxillofac Implants 2013;28(6):1589-601.

28. Funato A, Yamada M, Ogawa T. Success rate, healing time, and implant stability of photofunctionalized dental implants. Int J Oral Maxillofac Implants 2013;28(5):1261-71.

29. Aita H, Hori N, Takeuchi M, et al. The effect of ultraviolet functionalization of titanium on integration with bone. Biomaterials 2009;30(6):1015-25.

30. Suzuki S, Kobayashi H, Ogawa T. Implant stability change and osseointegration speed of immediately loaded photofunctionalized implants. Implant Dent 2013;22(5):481-90.

31. Suzuki T, Hori N, Att W, et al. Ultraviolet treatment overcomes time-related degrading bioactivity of titanium. Tissue Eng Part A 2009;15(12):3679-88.

32. Ogawa T. Ultraviolet photofunctionalization of titanium implants. Int J Oral Maxillofac Implants 2014;29(1):e95-102.

33. Ueno T, Yamada M, Suzuki T, et al. Enhancement of bone-titanium integration profile with

UV-photofunctionalized titanium in a gap healing model. Biomaterials 2010;31(7):1546-57.

34. Aita H, Att W, Ueno T, et al. Ultraviolet light-mediated photofunctionalization of titanium to promote human mesenchymal stem cell migration, attachment, proliferation and differentiation. Acta Biomater 2009;5(8):3247-57.

35. Att W, Hori N, Iwasa F, et al. The effect of UV-photofunctionalization on the time-related bioactivity of titanium and chromium-cobalt alloys. Biomaterials 2009;30(26):4268-76.

36. Iwasa F, Hori N, Ueno T, et al. Enhancement of osteoblast adhesion to UV-photofunctionalized titanium via an electrostatic mechanism. Biomaterials 2010;31(10):2717-27.

37. Att W, Ogawa T. Biological aging of implant surfaces and their restoration with ultraviolet light treatment: a novel understanding of osseointegration. Int J Oral Maxillofac Implants 2012;27(4):753-61.

38. Hori N, Ueno T, Minamikawa H, et al. Electrostatic control of protein adsorption on UV-photofunctionalized titanium. Acta Biomater 2010;6(10):4175-80.

39. Att W, Hori N, Takeuchi M, et al. Time-dependent degradation of titanium osteoconductivity: an implication of biological aging of implant materials. Biomaterials 2009;30(29):5352-63.

40. Hori N, Att W, Ueno T, et al. Age-dependent degradation of the protein adsorption capacity of titanium. J Dent Res 2009;88(7):663-7.

41. Kubo K, Att W, Yamada M, et al. Microtopography of titanium suppresses osteoblastic differentiation but enhances chondroblastic differentiation of rat femoral periosteum-derived cells. J Biomed Mater Res A 2008;87(2):380-91.

42. Kubo K, Tsukimura N, Iwasa F, et al. Cellular behavior on TiO2 nanonodular structures in a micro-to-nanoscale hierarchy model. Biomaterials 2009;30(29):5319-29.

43. Cooper LF. A role for surface topography in creating and maintaining bone at titanium endosseous implants. J Prosthet Dent 2000;84(5):522-34.

44. Harvey AG, Hill EW, Bayat A. Designing implant surface topography for improved biocompatibility. Expert Rev Med Devices 2013;10(2):257-67.

45. Stadlinger B, Pourmand P, Locher MC, et al. Systematic review of animal models for the study of implant integration, assessing the influence of material, surface and design. J Clin Periodontol 2012;39 Suppl 12:28-36.

46. Mendonca G, Mendonca DB, Aragao FJ, et al. Advancing dental implant surface technology-from micron- to nanotopography. Biomaterials 2008;29(28):3822-35.

47. Shalabi MM, Gortemaker A, Van't Hof MA, et al. Implant surface roughness and bone healing: a systematic review. J Dent Res 2006;85(6):496-500.

48. Goriainov V, Cook R, Latham JM, et al. Bone and metal: an orthopaedic perspective on osseointegration of metals. Acta Biomater 2014;10(10):4043-57.

49. Gongadze E, Kabaso D, Bauer S, et al. Adhesion of osteoblasts to a nanorough titanium implant surface. Int J Nanomedicine 2011;6:1801-16.

50. Klein MO, Bijelic A, Ziebart T, et al. Submicron scale-structured hydrophilic titanium surfaces promote early osteogenic gene response for cell adhesion and cell differentiation. Clin Implant Dent Relat Res 2013;15(2):166-75.

51. Yamada M, Miyauchi T, Yamamoto A, et al. Enhancement of adhesion strength and cellular stiffness of osteoblasts on mirror-polished titanium surface by UV-photofunctionalization. Acta Biomater 2010;6(12):4578-88.

52. Miyauchi T, Yamada M, Yamamoto A, et al. The enhanced characteristics of osteoblast adhesion to photofunctionalized nanoscale TiO_2 layers on biomaterials surfaces. Biomaterials 2010;31(14):3827-39.

53. Lee JH, Ogawa T. The biological aging of titanium implants. Implant Dent 2012;21(5):415-21.

54. Chang EJ, Kim HH, Huh JE, et al. Low proliferation and high apoptosis of osteoblastic cells on hydrophobic surface are associated with defective Ras signaling. Exp Cell Res 2005;303(1):197-206.

55. Hayashi R, Ueno T, Migita S, et al. Hydrocarbon deposition attenuates osteoblast activity on titanium. J Dent Res 2014;93(7):698-703.

56. Guo Z, Iku S, Mu L, et al. Implantation with new three-dimensional porous titanium web for treatment of parietal bone defect in rabbit. Artif Organs 2013;37(7):623-8.

57. Van der Stok J, Van der Jagt OP, Amin Yavari S, et al. Selective laser melting-produced porous titanium scaffolds regenerate bone in critical size cortical bone defects. J Orthop Res 2013;31(5):792-9.

58. Yoshinari M, Atsuzaka K, Kitazawa Y, et al. Properties of carbon-foam scaffold coated with titanium for tissue engineering. Biomedical Research 2003;24(4):195-203.

59. Hirota M, Hayakawa T, Ametani A, et al. The effect of hydroxyapatite-coated titanium fiber web on human osteoblast functional activity. Int J Oral Maxillofac Implants 2011;26(2):245-50.

60. Hirota M, Hayakawa T, Ametani A, et al. Use of the molecular precursor method to facilitate thin hydroxyapatite coating of titanium fiber web scaffold and enhance bone formation: an experimental study in rat cranial bone defects. Int J Oral Maxillofac Implants 2010;25(5):888-92.

61. Kuboki Y, Furusawa T, Sato M, et al. Bone enhancing effect of titanium-binding proteins isolated from bovine bone and implanted into rat calvaria with titanium scaffold. Biomed Mater Eng 2014;24(3):1539-48.

62. Ogawa T, Nishimura I. Different bone integration profiles of turned and acid-etched implants associated with modulated expression of extracellular matrix genes. Int J Oral

Maxillofac Implants 2003;18(2):200-10.

63. Ogawa T, Sukotjo C, Nishimura I. Modulated bone matrix-related gene expression is associated with differences in interfacial strength of different implant surface roughness. J Prosthodont 2002;11(4):241-7.

64. Datta N, Pham QP, Sharma U, et al. In vitro generated extracellular matrix and fluid shear stress synergistically enhance 3D osteoblastic differentiation. Proc Natl Acad Sci U S A 2006;103(8):2488-93.

65. Wenzel R. Resistance of solid surfaces to wetting by water. J Ind Engineering Chem 1936;28(8):988-94.

66. Frisch SM, Ruoslahti E. Integrins and anoikis. Curr Opin Cell Biol 1997;9(5):701-6.

67. Tian YS, Kim HJ, Kim HM. Rho-associated kinase (ROCK) inhibition reverses low cell activity on hydrophobic surfaces. Biochem Biophys Res Commun 2009;386(3):499-503.

68. Glimcher MJ. Mechanism of calcification: role of collagen fibrils and collagen-phosphoprotein complexes *in vitro* and *in vivo*. Anat Rec 1989;224(2):139-53.

69. Nancollas GH, LoRe M, Perez L, et al. Mineral phases of calcium phosphate. Anat Rec 1989;224(2):234-41.

70. Hirota M, Hayakawa T, Yoshinari M, et al. Hydroxyapatite coating for titanium fibre mesh scaffold enhances osteoblast activity and bone tissue formation. Int J Oral Maxillofac Surg 2012;41(10):1304-9.

71. van den Dolder J, Vehof JW, Spauwen PH, et al. Bone formation by rat bone marrow cells cultured on titanium fiber mesh: effect of *in vitro* culture time. J Biomed Mater Res 2002;62(3):350-8.
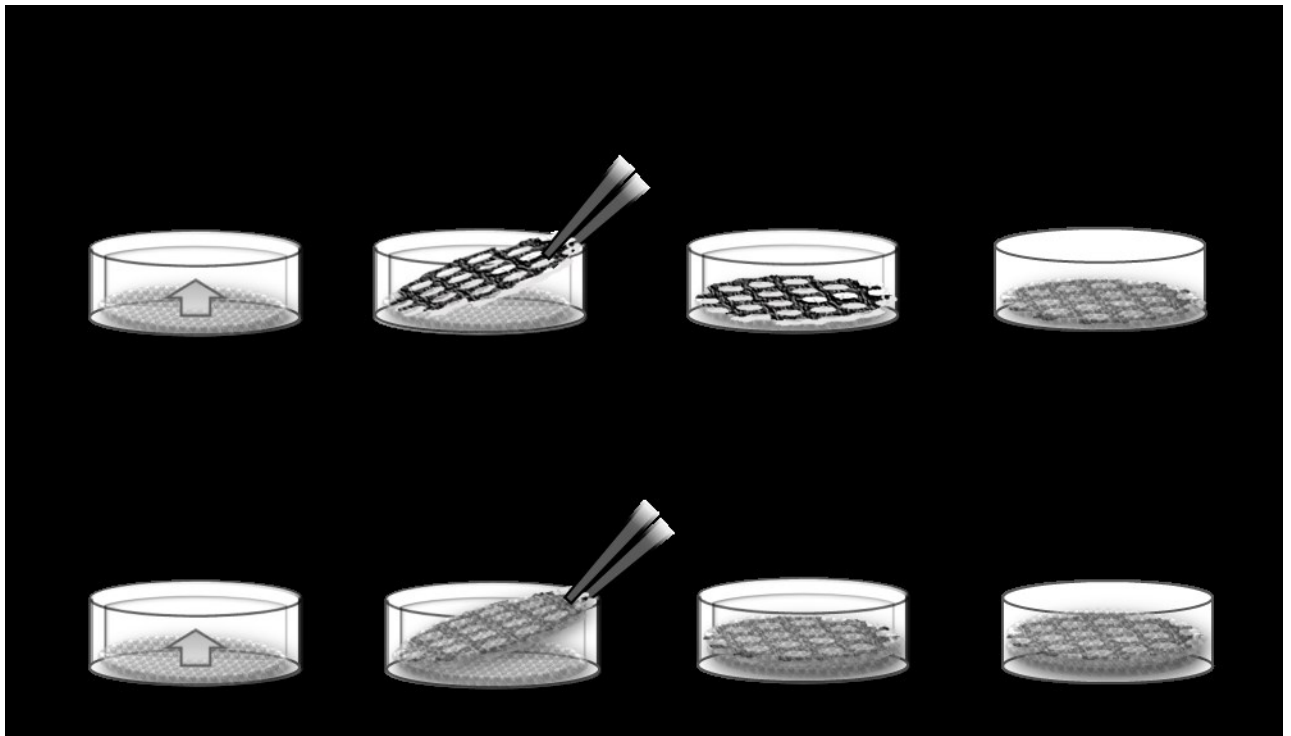
Figure 1
Step-by-step protocols of titanium-reinforced osteogenic cell sheet construction using two different methods: single-sided and double-sided. Micro-thin (50 μm thick) titanium plates with apertures were cut into circles (5 mm diameter) and acid-etched with H_2SO_4 prior to use, and then used either untreated or after photofunctionalization.
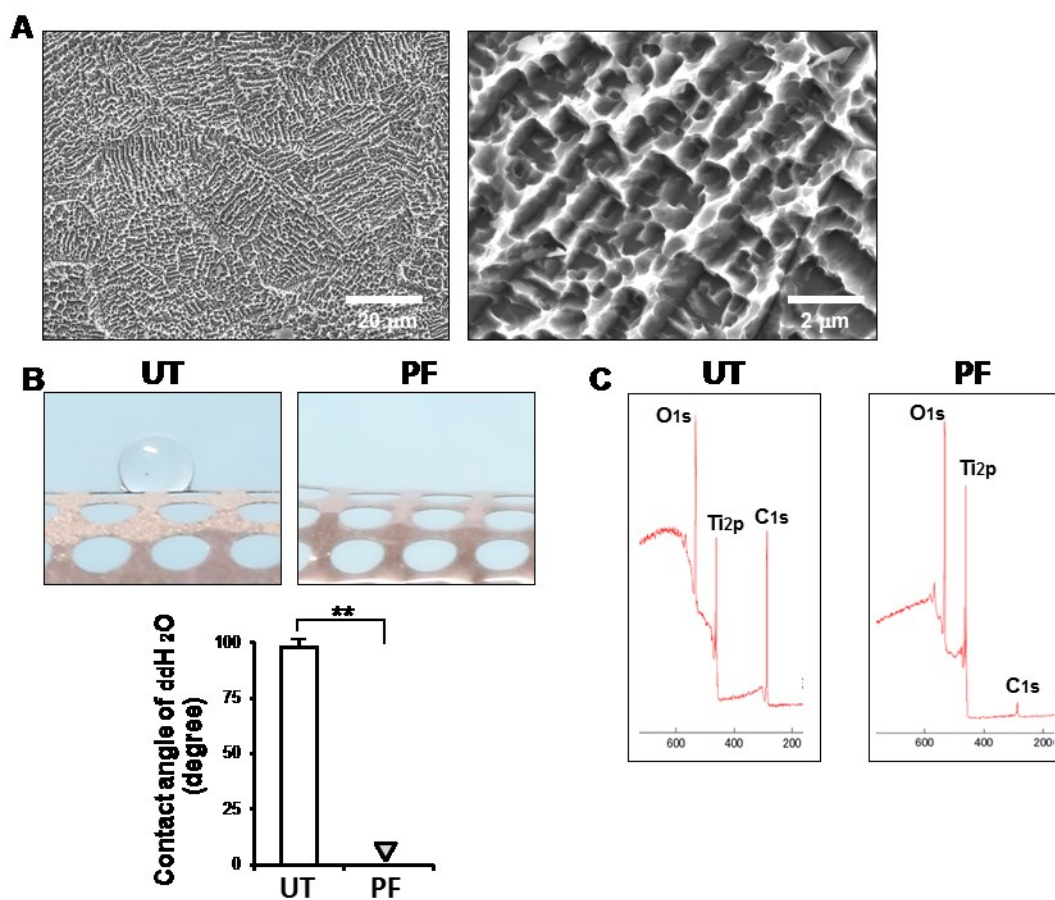
Figure 2

Surface characterization of the titanium plates used in this study. (A) Surface morphology. Low- (left) and high- (right) magnification SEM images of the titanium surface. (B) Wettability assay. Side-view images of 10 μl of ddH$_2$O droplets placed on untreated (UT) and photofunctionalized (PF) titanium plates, along with the measured contact angle. **$p < 0.01$. (C) XPS spectra for untreated and photofunctionalized titanium plates.
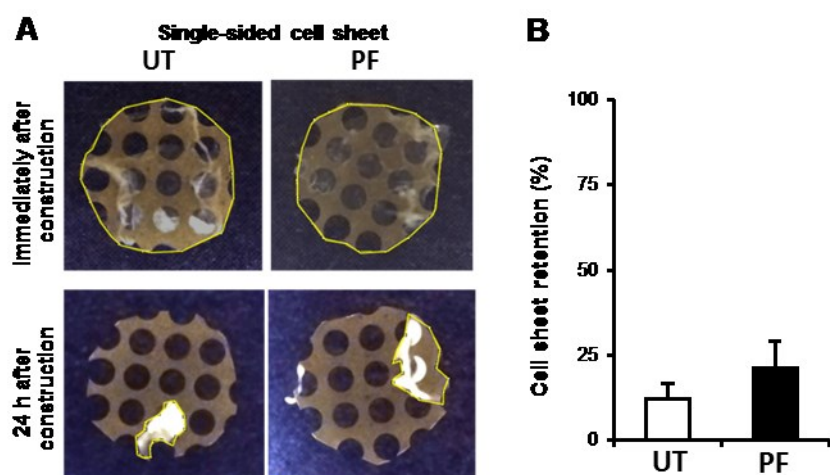
Figure 3

Retention or dissociation of a cell sheet attached to a titanium plate. A single cell sheet layer was attached to an untreated (UT) or photofunctionalized (PF) titanium plate. (A) Photographic images of a cell sheet on a titanium plate immediately and 24 h after titanium-cell sheet complex construction. (B) Mean and standard deviation of cell sheet retention (%) measured as [(area of cell sheet coverage 24 after construction) / (area of cell sheet coverage immediately after construction)]×100.
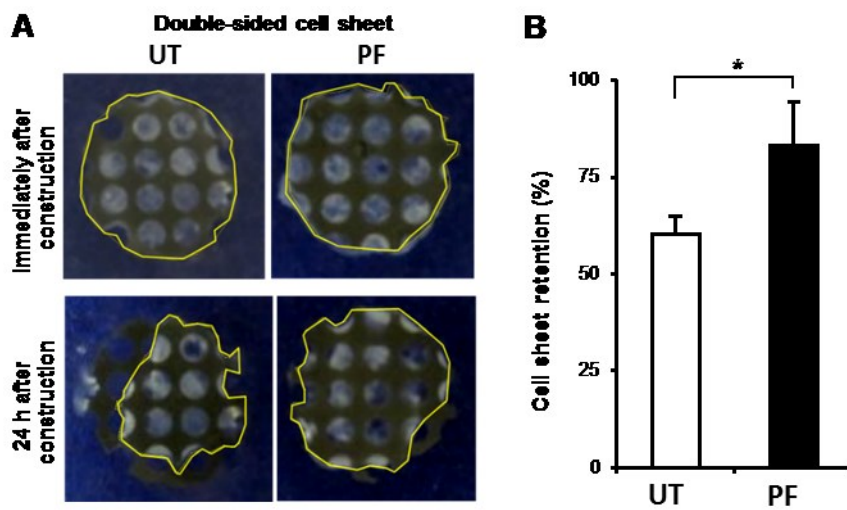
Figure 4

Retention or dissociation of double-sided cell sheets attached to a titanium plate. Titanium plates were either untreated (UT) or photofunctionalized (PF). (A) Photographic images of cell sheets immediately and 24 h after titanium-cell sheet complex construction. (B) Mean and standard deviation of cell sheet retention (%) measured as [(area of cell sheet coverage 24 after construction) / (area of cell sheet coverage immediately after construction)] × 100. *$p < 0.05$.
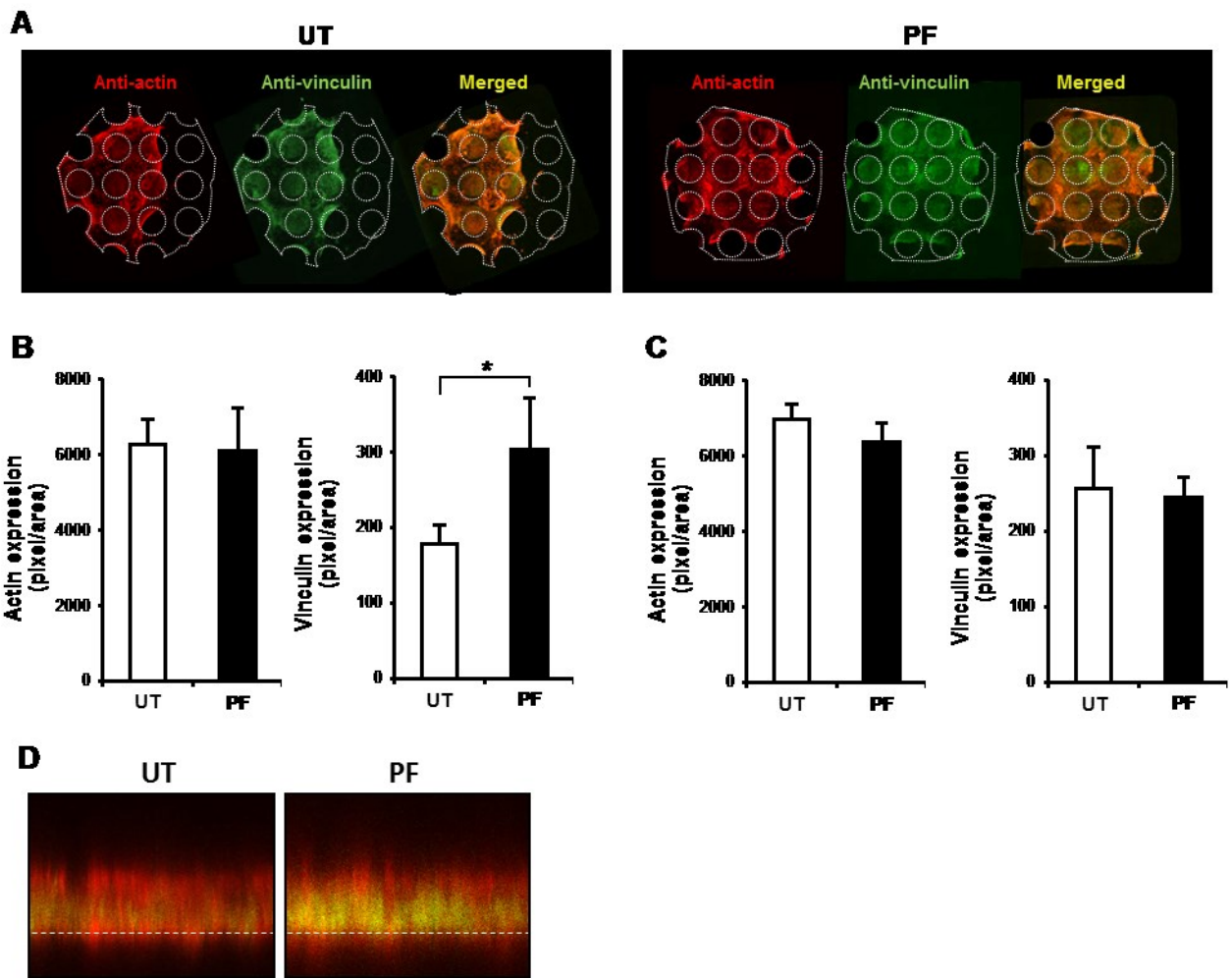
Figure 5

Cell sheet-titanium integrity 24 h after construction. Double-sided cell sheets constructed with untreated (UT) and photofunctionalized (PF) titanium plates were assessed. (A) Confocal microscopic images of cell sheets with immunochemical staining for cytoskeletal actin and vinculin are shown. (B, C) Densitometric evaluation of the expression of actin and vinculin on the titanium frame (B) and within apertures (C). $*p < 0.05$. (D) Typical cross-sectional confocal microscopic images of the cell sheet-titanium interface stained with actin and vinculin. The upper border of the titanium framework is indicated with a dotted line. Note the high intensity of green (vinculin) on the photofunctionalized titanium frame.
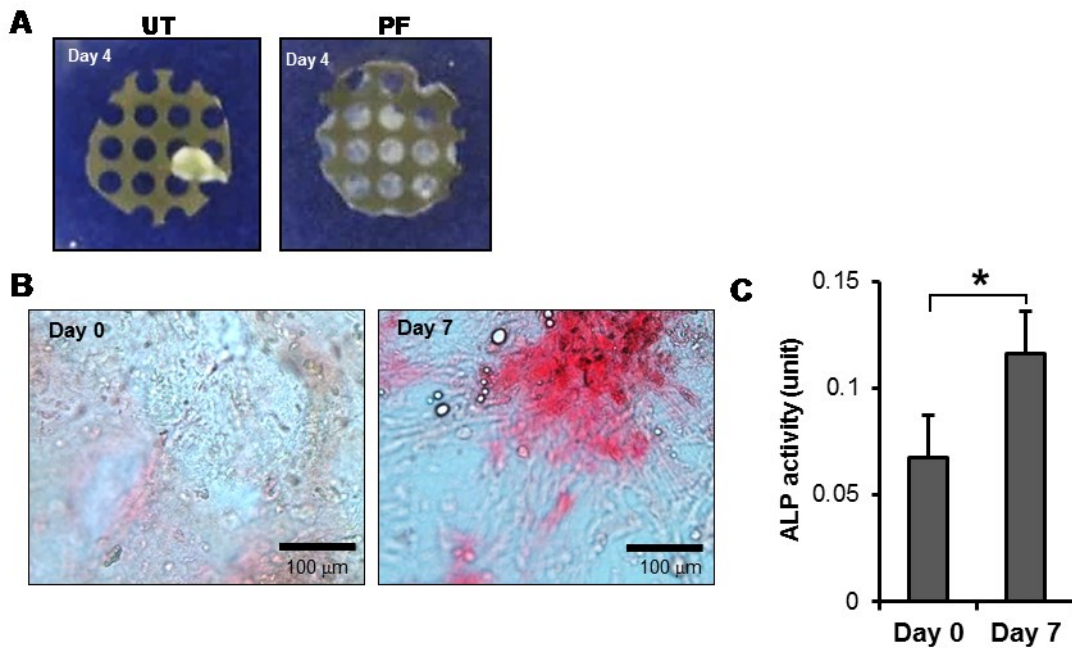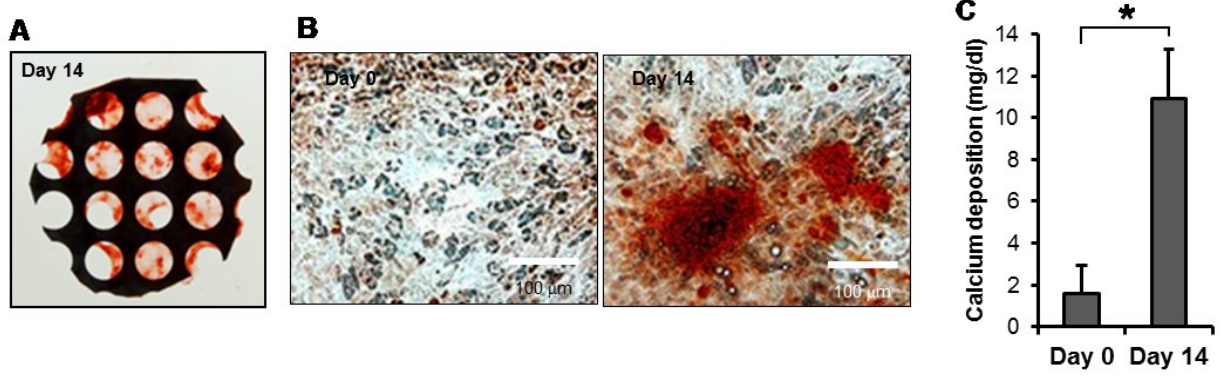
Figure 6

Osteogenic functional phenotypes on titanium-reinforced cell sheets. Double-sided cell sheets constructed with photofunctionalized titanium framework were analyzed. (A) Photographic images of the double-sided cell sheets constructed with untreated (UT) and photofunctionalized (PF) titanium frameworks after four days of incubation. (B) Microscopic images of double-sided cell sheets constructed with a photofunctionalized titanium framework at days zero and seven after alkaline phosphatase (ALP) staining. (C) Colorimetric detection of ALP activity for the double-sided cell sheets constructed with photofunctionalized titanium. $*p < 0.05$.

Figure 7

Osteogenic mineralization on titanium-reinforced cell sheets. Double-sided cell sheets constructed with photofunctionalized titanium were analyzed.   (A) A photographic image of the double-sided cell sheets constructed with photofunctionalized titanium after 14 days of incubation. (B) Microscopic images of double-sided cell sheets with photofunctionalized titanium stained with Alizarin red at days 0 and 14 of culture. (C) Colorimetric detection of calcium deposition measured on the same days of culture. *$p < 0.05$.
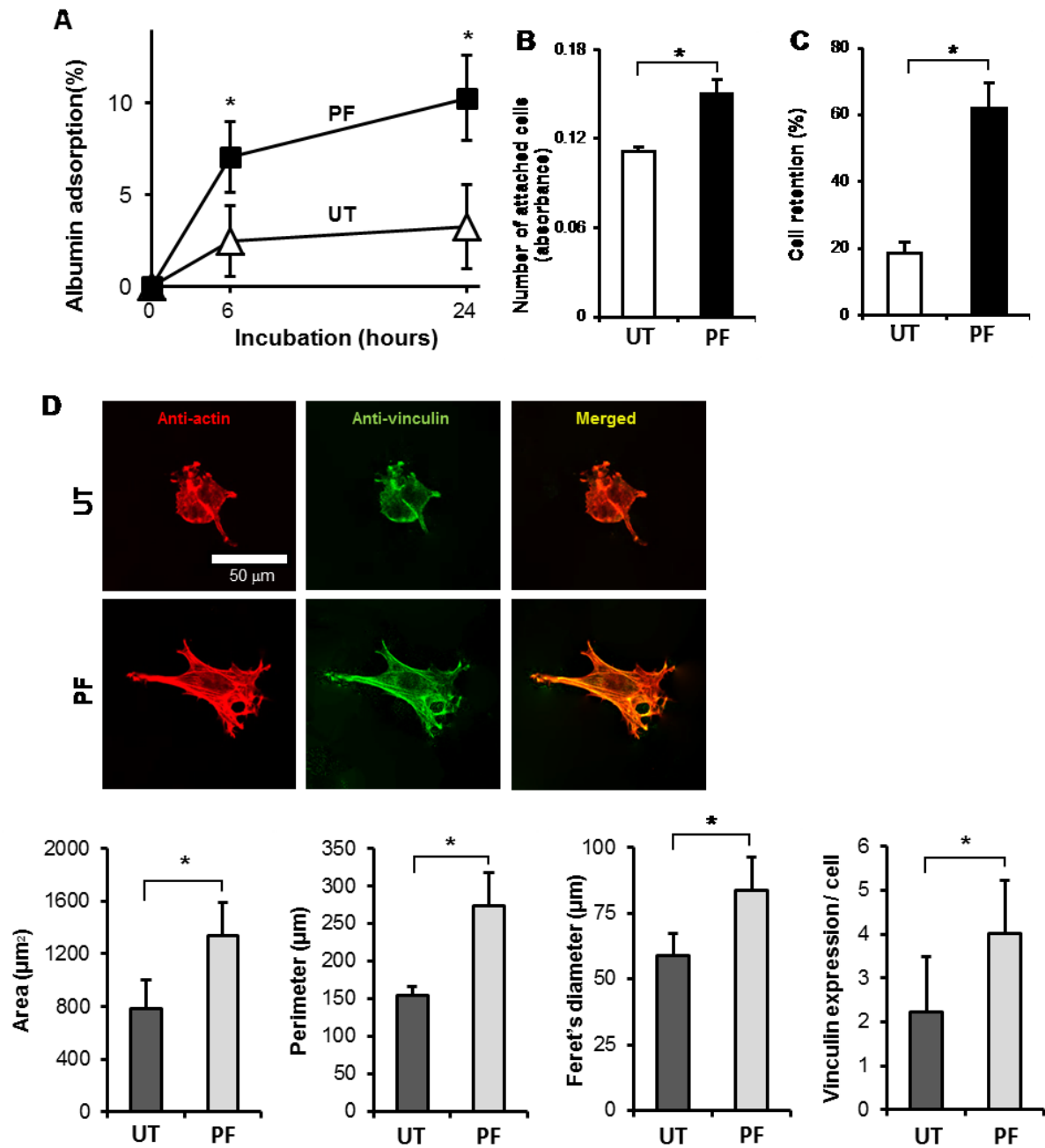
Figure 8

Biological characterization of photofunctionalized titanium frames. (A) Albumin adsorption to untreated (UT) and photofunctionalized (PF) titanium frames during six and 24 h of incubation. (B) Number of periosteal cells attached after 24 h incubation. (C) The percentage of cells retained on titanium frames after chemical and mechanical detachment. Cells settled on titanium frames for 24 h were detached. (D) Confocal microscopic images of periosteal cells cultured on untreated and photofunctionalized titanium frames for 24 h, with immunochemical staining for actin and vinculin shown; cytomorphometric and densitometric parameters are also shown. *$p < 0.05$.
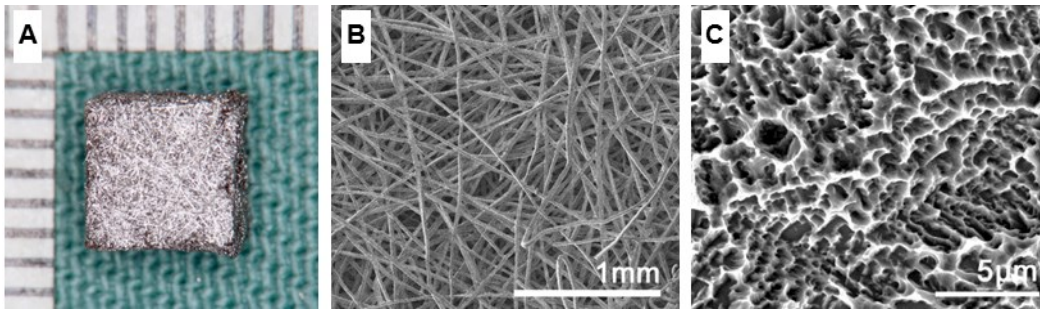
Figure 9

(A) Titanium scaffolds comprising thin fibers were 5 mm×5 mm and 3 mm thick, with a porosity of 89 %. (B, C) Scanning electron microphotographs of the titanium scaffolds and the surface topography of the titanium wire.
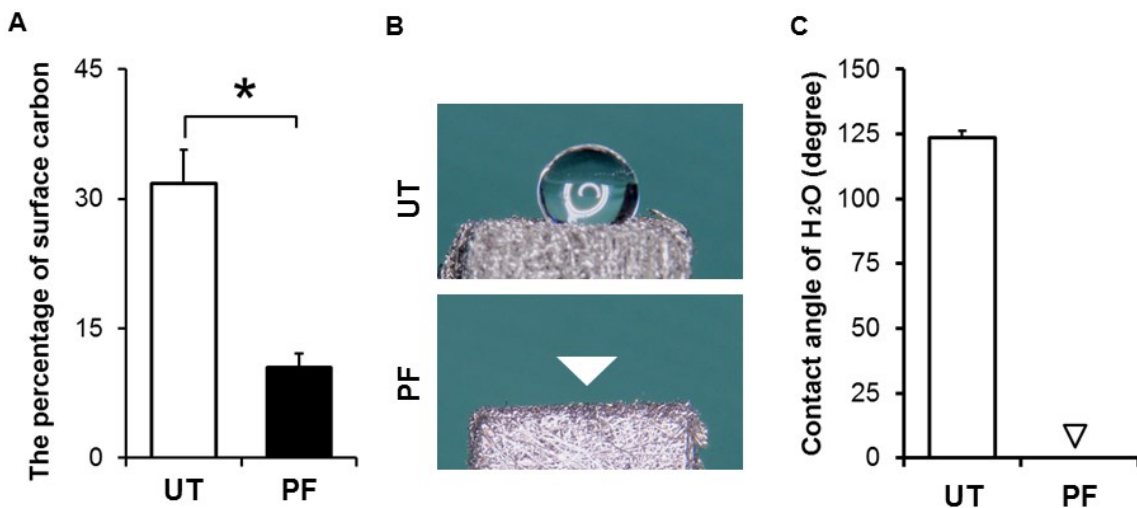

Figure 10

Photofunctionalization induced physicochemical changes on titanium scaffolds. (A) The percentage of surface carbon on titanium scaffolds. Untreated (UT) and photofunctionalized (PF) scaffolds. * $p < 0.05$. (B) Side-view images of 10 μl of water droplets placed on the untreated control titanium scaffolds and photofunctionalized scaffold to test their wettability (the arrow represents the place where the water drop was placed). (C) The graph shows the contact angle of dropped water with an arrow representing a 0° of contact angle in the photofunctionalized scaffolds.
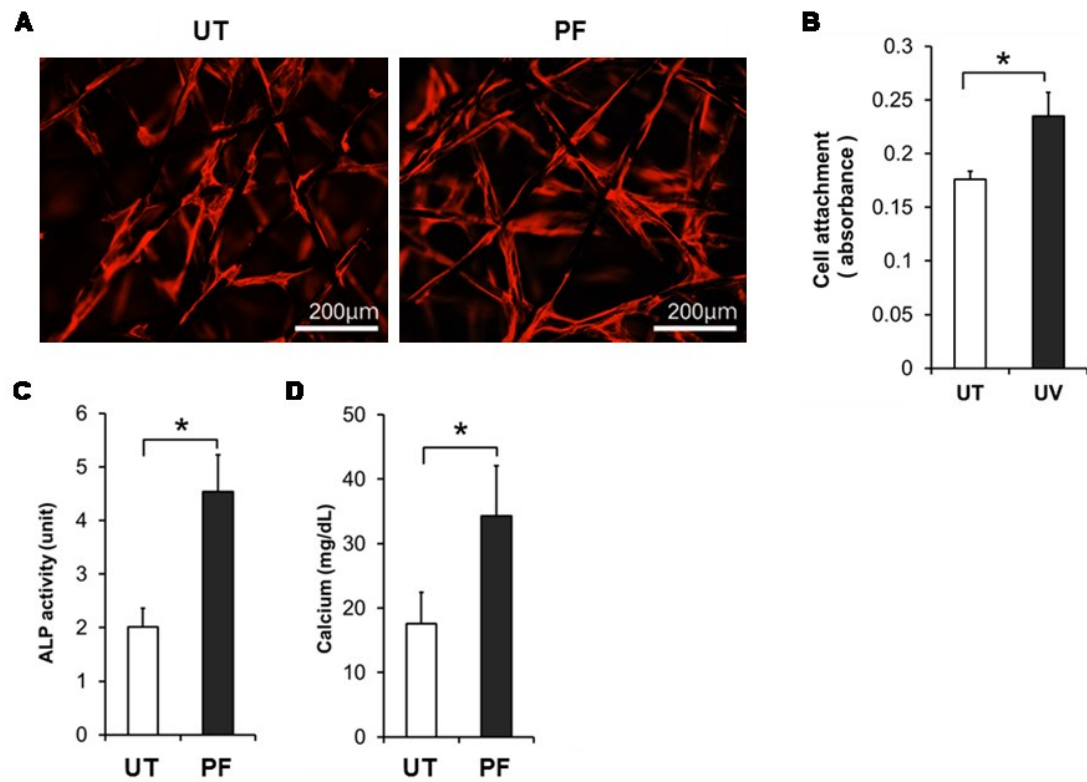
34

Figure 11

Increased number of attaching cells and enhanced osteoblastic phenotype on the photofunctionalized scaffold. (A) Micrograph of osteoblasts cultured on scaffold 24 h after seeding (actin filaments are represented in green). Untreated control titanium scaffolds (UT) and photofunctionalized scaffold (PF). (B) The number of cells was measured colorimetrically with WST-1 reagent 24 h after seeding. (C) The activity of alkaline phosphatase (ALP) was quantified colorimetrically. (D) The amount of calcium deposition was quantified colorimetrically. * $p < 0.05$.
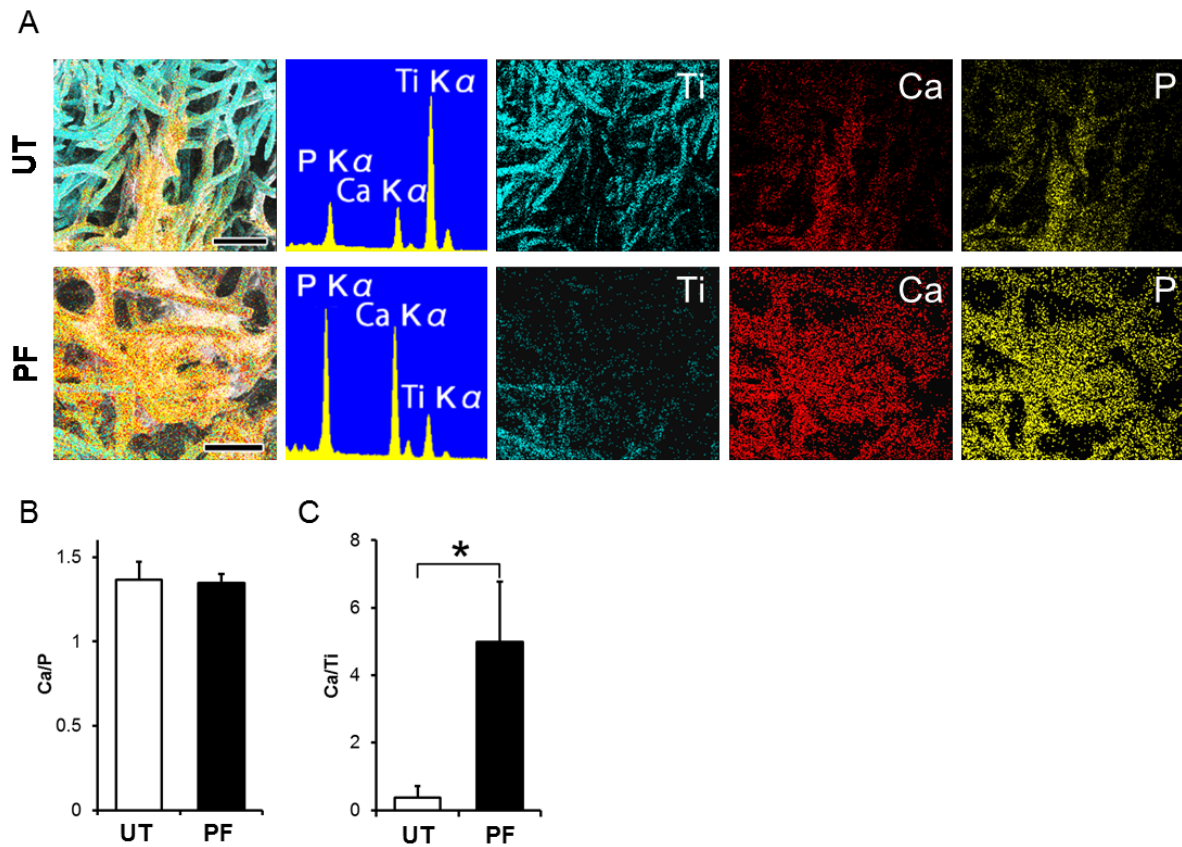
Figure 12

Enhanced bone formation on the photofunctionalized scaffolds. (A) The mapping images and spectrums of energy dispersive x-ray spectroscopy surface element analysis of biological structures formed on untreated control scaffolds (UT) and photofunctionalized scaffolds (PF) [titanium (cyan), calcium (red), and phosphorus (yellow)]. Scale bar represents 100 μm. (B) Ca/P ratio of biological structures formed on the scaffolds. (C) Ca/Ti ratio of biological structures formed on the scaffolds. $* p < 0.05$.
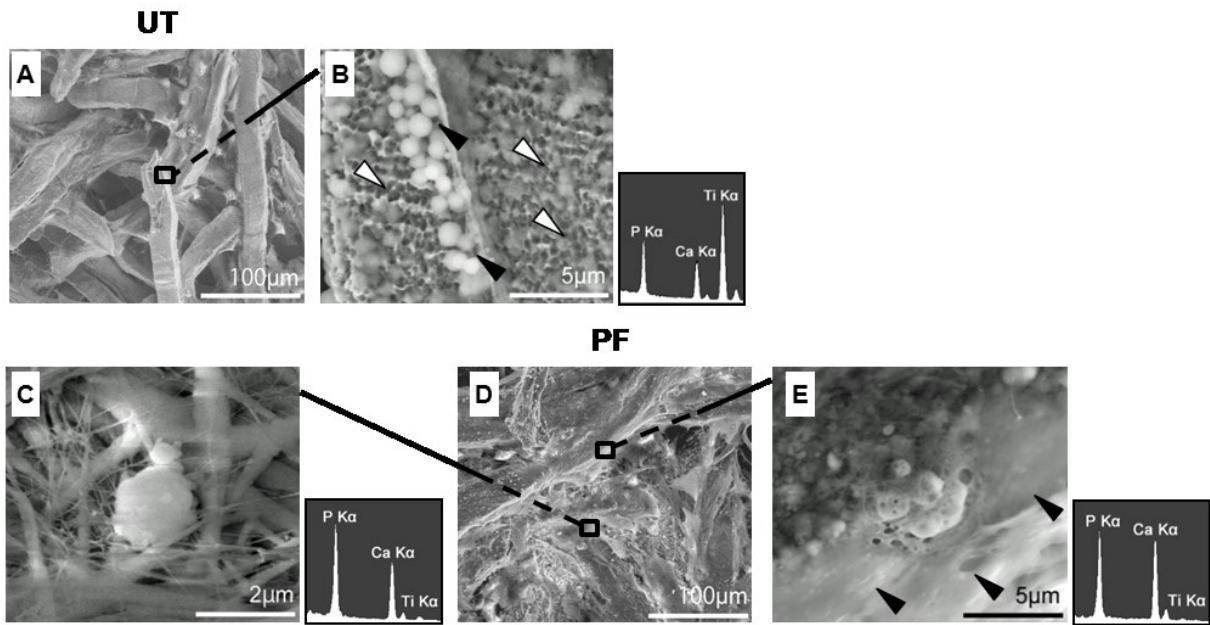
Figure 13

Enhanced formation of calcified structures with extracellular matrix on the photofunctionalized scaffolds. (A) Untreated control scaffolds (UT) showed a clear existence of titanium fibers with few attaching cells in the low magnification image. (B) Control untreated scaffolds showed exposed bear titanium surfaces (white arrows) with matrix vesicle secreted by osteoblasts (black arrows). (C) Photofunctionalized scaffolds (PF) showed collagen-like fibers with matrix vesicles between titanium fibers. (D) Photofunctionalized scaffolds showed scaffolds almost fully covered by biological structures and the existence of extracellular matrix filling the space between titanium fibers in the low magnification image. (E) The surface of fibers in photofunctionalized scaffolds was fully covered by the structure comprising calcium and phosphorus.